Plastic Deformation and Modification of Surface Characteristics in Nano and Micro Levels and Enhancement of Electric Field of FCC Materials Using Cavitaion Phenomenon

Ezddin Hutli[1*], Attila Bonyár[2], Daniel Oszetzky[3], Milos S. Nedeljkovic[4]

[1*] – Ph.D., Department of Thermohydraulics, Centre for Energy Research, Hungarian Academy of Sciences, Budapest-Hungary-University of Belgrade, Faculty of Mechanical Engineering
ezddinhutli@yahoo.com
[2] – Assistant Professor, Ph.D., Budapest University of Technology and Economics, Department of Electronics Technology
[3] –Ph.D., Scientific Co-Worker, Department of Applied and Nonlinear Optics, Institute for Solid State Physics and Optics, Wigner RCP of the H.A.S.
[4] – Professor, Ph.D., University of Belgrade, Faculty of Mechanical Engineering

Abstract
The aim of this paper is to demonstrate and establish a possible application of the cavitation phenomenon as an efficient method to modify surface properties. Three FCC (Face Centered Cubic) materials were subjected to high speed submerged cavitating jets under certain working conditions, for time periods between 15 and 1,800 s. The force generated by cavitation is employed to modify the surface roughness in nano and micro scales. The target surface was investigated with digital optical microscopy, atomic force and electrostatic force microscopy (AFM and EFM) and also with a white light interferometer. These different observation techniques indicate that at short exposure times, the observed characteristic features in the microstructure – hills, holes and wavy configuration – can be related to the start of the plastic deformation of the specimen surface. Longer exposure times inevitably result in a greater number of jet specimen interactions leading to specimen erosion and fracture. The results demonstrate the possibility to use cavitation bubbles as a micro- nanofabrication method for the surface preparation/modification or shoot-less surface peening. EFM results present a possibility of using cavitation as tool to enhance the electrostatic properties of a metal surface by modifying its roughness. The degree of enhancement depends on the material properties.

Key words: microstructure, roughness, EFM, electrostatic, cavitation, plastic deformation

1. Introduction

Cavitation is generally considered to be an undesired, sometimes even harmful phenomenon in hydraulic systems. It was first discovered and investigated theoretically as a physical phenomenon, by Reynolds O. in 1873. Inertial cavitation was first studied by Lord Rayleigh in the late 19th century [1].

Cavitation phenomenon is a process, which is characterized by small bubbles or large "cavities", which appear and grow when and where the pressure drops below the vapour pressure of the liquid at a given temperature. Pressure recovery causes these bubbles to implode in a few microseconds. These implosions or collapses generate pressure shockwaves, micro liquid jets and noise. These implosions can be so violent that they produce local permanent deformation and rupture of the materials in its vicinity. Moreover, if cavitation replaces a large volume of the liquid in a machine, a drop in efficiency could be the result. These side effects (noise, vibration, erosion and performance drop), explain why this research field is important for hydraulic systems [2-6]. On the other hand, cavitation can widely be used in many areas such as industrial cleaning applications, since cavitation has sufficient power to overcome the particle-to-substrate adhesion forces to loosen contaminants. It also plays an important role in the chemical engineering industry (homogenization, mixing and breaking down processes). In the biomedical field cavitation is used for the destruction of kidney stone and there are also numerous attempts to apply it for the non-thermal and non-invasive fractionation of tissue for the treatment of a variety of diseases. It may also be used in High-Intensity Focused

Ultrasound (HIFU) to locally heat and destroy diseased or damaged tissue through ablation. In the engineering industry cavitation impact is also utilized to modify surfaces in the same way as shot peening, for example, it could be used to improve the fatigue strength. Soyama H, et al. [3] have already demonstrated the enhancement of compressive residual stress, the improvement of the fatigue strength of metallic materials, and an improvement in corrosion resistance by using a normal cavitating jet in water. He also reported in another work that the fatigue strength of a specimen peened by a cavitating jet is considerably improved compared to a shot peened specimen by using a rotational bending fatigue test [4]. Therefore the possibility of using cavitation phenomenon as tool to modify the surface and to improve the material properties sheds a positive light onto this phenomenon which explains the increased investigation activity in this area too.

In order to provide a greater understanding of the cavitation-solid interaction phenomenon, a number of different testing techniques have been used by researchers to investigate the different cavitation damage stages. Still, this subject is in the focus of active investigation, especially, when new technologies are used. Examples of available techniques are the pit-count technique, the 2D optical method, the 3D measurements by roughness meter, and the 3D laser profilometry technique [7]. As well known, the surface roughness is an important factor when dealing with issues such as cavitation collapse on the surface, friction, lubrication, and wear. It also has a major impact on applications involving thermal or electrical resistance, fluid dynamics, noise and vibration control, dimensional tolerance, and abrasive processes, etc. [8]. Surface roughness of metals which are used in the medical field as implants fixed to the bone is an important factor in the recovery process of the patient, because it affects osseointegration. It is reported that increased micro/submicron roughness could enhance the bone cell function [9]. The micro roughness of the solids plays the main role for the heat transfer in a cross interface, which is an important phenomenon existing in a wide range of applications, such as microelectronics cooling, spacecraft structures, satellite bolted joints, nuclear engineering, ball bearings, and heat exchangers. The heat transfer mode at the micro contact is conduction, which leads to high temperature drop across the interface [10]. Changes in the surface roughness also influence the electrostatic field above a biased sample. In electrostatics the intensity of the electric near filed is higher above structures with small geometrical curvature (e.g. sharp features). Such perturbed and intensive near fields could be desirable for some applications [11]. Surface roughness could exert a profound effect on the performance of radio-frequency (RF) cavities or slow wave structures [12-14]. Surface roughness may lead to excessive local electric field enhancement that could trigger RF breakdown [15, 16]. Surface roughness may also cause local magnetic field enhancement which can lead to abrupt quenching i.e. loss of superconductivity [12, 17].

Considering the above mentioned points, the surfaces with nano and micro scales of roughness, with regular or irregular shape, wavy or stripped shape etc. are assumed to be important targets for research. Therefore, the primary aim of this work was to experimentally determine the initiating mechanism at the start of the cavitation damage and the erosion process in FCC materials (namely Al-alloy, Cu and SS316 as a tested materials, or targets); and then secondly, to investigate the behavior of the target material during and after the incubation time period by using nanometrology tools (such as AFM) in order to demonstrate the possibility of using the cavitation phenomenon as tool to test and modify the surface properties in a micro and nano level (roughness and/or waviness). The white light interferometric surface analyzer was used in this work as an experimental tool which provided additional insight into the deformation process. To investigate the effect of the surface roughness on the electrostatic properties of the sample electrostatic force microscopy (EFM) was used.

2.Methodology and experimental procedure

Series of tests were carried out involving repeated exposure of the tested specimens of FCC materials to the action of a cavitating water jet for given time periods. Fig. 1. shows the schematic diagram of the test chamber and a photo of how the cavitating jet impacts the specimen. The working fluid used in the experiments was tap water. It was not degassed, hence it is expected to be saturated with dissolved air. This gas content has not been measured.

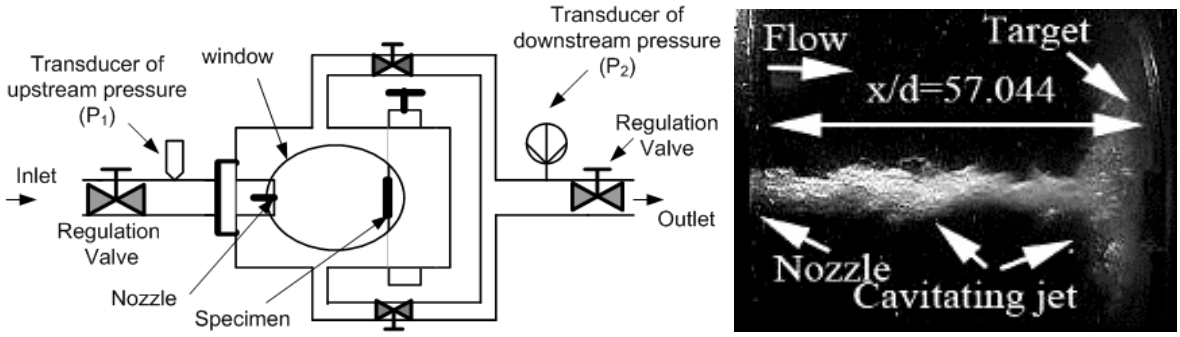

Figure 1. Schematic diagram of the test chamber and a photo of how the cavitating jet impacts the specimen. (x/d: non-dimensional stand-off distance, where x is the distance between the nozzle outlet and the sample surface and d is the nozzle diameter)

In order to have a good control over the cavitation intensity, the upstream pressure (P_1) and downstream pressure (P_2) were measured at the inlet and outlet of the test chamber, respectively, as shown in Fig.1. The pressure transducers were calibrated by the manufacturer and accuracy certificates were issued for a maximum error of +0.2/-0.21 % FS (Full Scale). The flow rate (exit jet velocity) was determined by using P_1 and P_2 values from the previous nozzle calibration, the uncertainty of its determination is also in the range of +/- 0.3 % FS.

The exposure times were chosen in a way that the level of damage on each specimen would not exceed the plastic deformation level – i.e the exposure time is less than or equal to the incubiation time of the target materials. The surface roughness and surface characteristic of the specimen before and after the cavitation damage test was investigated. Before the tests, specimens were prepared by polishing, in order to provide a smooth surface for the examination of cavitation damage in detail. Before the analysis of a tested sample, it was cleaned, dried and placed in the desiccator at ambient conditions. More information regarding the sample preparation and the control of cavitating jet parameters can be found in our previous works [18-20].

3.Tested Materials

The surface modification (damage), produced by impingement of a cavitating jet, was investigated experimentally using three basic kinds of tested materials: aluminum alloy (AlSiMg,Al-alloy containing Mn = 1.07, Mg = 0.76, Si = 1, Fe = 0.39 in weight %), stainless steel (SS.316 containing 18 % Cr and 10 % Ni), and copper (Cu – commercial purity), with water as a working fluid in the temperature range of 19-20 ^{o}C. These materials were selected to cover face centered cubic structures like steel and non-ferrous materials with either single phase (Cu) or multiphase structures (Al alloy). Table 1 collects the test conditions. The specimens have a disc shape with 14 mm diameter and 2.98 mm thickness. The featured (rings) of cavitation damage could be obtained on a metallic specimen surface by using a highly submerged cavitating jet with conical nozzle. The cavitation number (σ) and average exit jet velocity (V_J) are calculated as presented in previous works [18-20].

Fig. 2 shows the surface topography of the Al-alloy, Cu and SS316 specimens respectively, observed before the tests (as a reference, before the cavitation attack) measured by atomic force microscopy (AFM).

Table 1: Hydrodynamic and geometrical conditions applied in the experiments. All the test conditions resulted in plastic deformation of the samples excluding the two marked by *, where erosion of the sample was also occurred.

Tested Material	Exposure-time (t) [sec]	Nozzle geometry & (X/d)[-]	P_1 [bar]	P_2 [bar]	V_J [m/s]	σ [-]
Al-alloy	15	Convergent (X/d=57)	167±1	3.04±0.01	157±0.5	0.025 ± 0.001
Al-alloy	20	Convergent (X/d=57)	167±1	3.04±0.01	157±0.5	0.025 ± 0.001
Al-alloy	30	Convergent (X/d=57)	159±1	3.45±0.01	153±0.5	0.029±0.001
Cu(pure)	15	Convergent (X/d=57)	159±1	3.45±0.01	153±0.5	0.029±0.001
Al-alloy*	1800	Convergent (X/d=57)	145±1	2.1±0.1	147±0.5	0.0193±0.001
Cu(pure)*	1800	Convergent (X/d=57)	145±1	2.1±0.1	147±0.5	0.0193±0.001
Cu(pure)	600	Divergent(X/d=25.67)	157±1	2.1±0.1	23.5±0.5	1.042±0.001
St.St.316	1800	Convergent (X/d=57)	145±1	2.1±0.1	147±0.5	0.0193±0.001

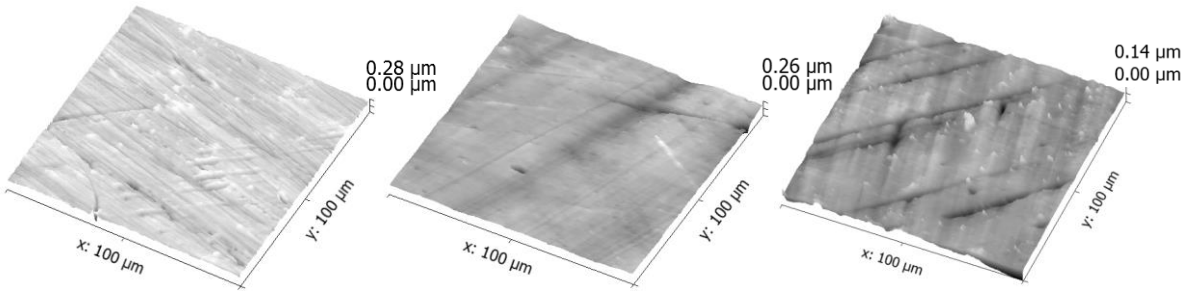

Figure 2. Surface topography measured before the tests (as a reference, before the cavitation attack) by atomic force microscopy (AFM). From left to right Al-alloy, Cu and SS316, respectively.

4.Measurement techniques

4.1.Digital Microscopy

A Hirox KH 7700 high speed digital microscope was used to image the surface of the specimens after long exposure times (1800 s). Besides the high optical resolution and wide field of view the advantage of this microscope is the variable angle of view, which can be beneficial for the investigation of cavitation damage [21]. Sample digital microscopy results are presented in Fig. 3.

4.2.White light interferometry

To measure the surface properties of the plastically deformed specimens a Zygo New View 7100 white light interferometer was used. Since the whole damaged area is much too large to measure it in one step with the required resolution, multiple images were made on the circular symmetric areas of plastic deformation as can be seen on Fig. 3. The center of jet impact was used as a reference point for every sample and the topography was measured in given distances (0, 1.5, 2, 3, 4 and 6 mm) from this point along 3 axis. The distribution of results on the sample surface can be seen on Fig. 6, the exact location of the measurements are also presented in Table 2. For this purpose objective lenses with a magnification of 50x and 10x were used. The resulting images have a vertical resolution of 0.1 nm for both lenses with lateral resolutions of 300 nm and 1.5 µm and scan sizes of 0.14 mm * 0.19 mm and 0.7 mm * 0.94 mm for the 10x and 50x lenses respectively.

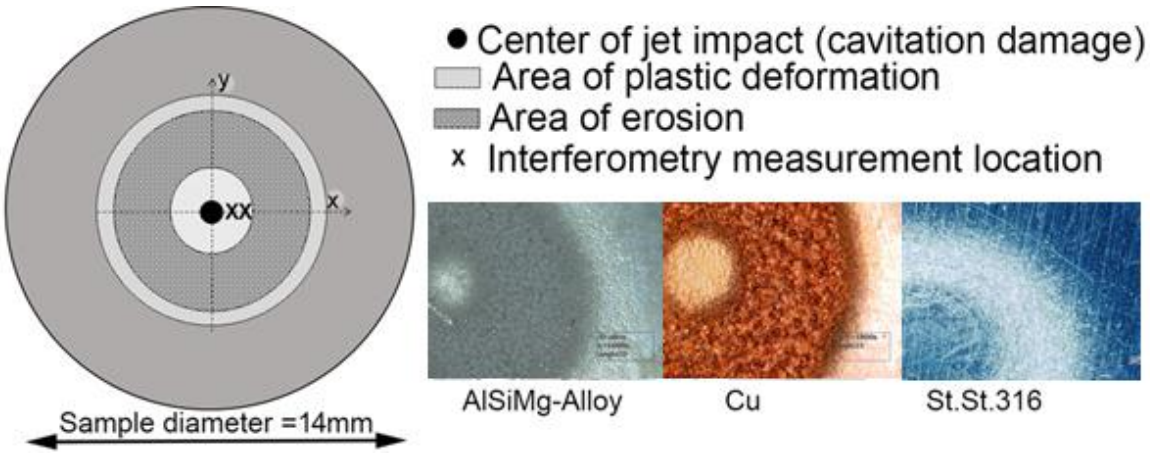

Figure 3. Illustration of the cavitation damage pattern (center of jet impact, plastic deformation and erosion stage). Note that 1) the center of impact is not always the same as the center of the sample; 2) the radius of the ringed areas are depending on the exposure time; 3) the appearance of other areas is possible. The presented digital images were obtained after long term exposure (1800 s) on Al-alloy, SS316 and Cu samples, respectively (the working conditions are presented in Table 1).

Surface roughness (S_a, S_{RMS}) and skewness (S_{sk}) values are calculated based on the following definitions (Equations 1-3), where η_i is the vertical distance from the mean plane to the z_i height of a scanned point, N is the total number of points and μ_n is the nth central moment calculated for the distribution of height points. Skewness characterizes the symmetry of the height distribution and can yield useful information from rough surfaces e.g. to differentiate between the dominant features (for example: a generally flat surface with some hills on it will have a positive skewness, a flat surface with holes will have negative skewness, while a balanced roughness has small absolute skewness).

$$S_a = \frac{1}{N}\sum_{i=1}^{N}|\eta_i| \qquad (1)$$

$$S_q = \sqrt{\frac{1}{N}\sum_{i=1}^{N}\eta_i{}^2} = \mu_2^{1/2} \qquad (2)$$

$$S_{sk} = \frac{\frac{1}{N}\sum_{i=1}^{N}\eta_i{}^3}{(\frac{1}{N}\sum_{i=1}^{N}\eta_i{}^2)^{3/2}} = \frac{\mu_3}{\mu_2^{3/2}} \qquad (3)$$

4.3 Scanning Probe Microscopy (SPM):

Atomic force microscopy (AFM) and electrostatic force microscopy (EFM) measurements were done with a Veeco (lately Bruker) diInnova type SPM. During EFM the microscope was operated in dynamic lift mode with 500 mV bias and 20 nm lift distance between the tip and the sample. Bruker SCM-PIT probes were used, which have 75 kHz nominal resonance frequency and 2.8 N/m nominal spring constant. The probe has an electrically conductive tip ensured by the platinum-iridium coating. The 100 µm x 100 µm EFM images were recorded with 512 x 512 sampling rate and 1 Hz scan rate. The PID values were optimized according to the user manual. For data evaluation the freeware

Gwyddion 2.27 software was used. All AFM and EFM measurements were performed at laboratory ambient temperature and with vibration filtering [23].

5.Results and Discussion:

5.1. Interferometry and AFM results

Prior to the cavitation experiments AFM measurements were done on the polished surfaces, which are presented in Fig 2. As can be seen, the surfaces are flat with only some minor scratches originating from the polishing. Fig.3. shows the cavitation damage pattern (plastic deformation and/or erosion stage) as an illustration and also on digital microscopy images obtained after long term tests (1800 s) on Al-alloy, Cu and SS316 samples. It can be seen, that the areas related to plastic deformation and erosion are circular in shape and centered around the impact point of the jet. The radius of these areas are depending on both the material properties and the exposure time. It can clearly be seen on the images, that the previously flat surface became wavy and rough, implying the presence of hills and holes (pits) in a circular pattern.

The results of the surface characterization with the white light interferometer are presented in Figures 4, 5 and 6. Fig. 4 compares the effect of cavitation in the case of the Al-alloy sample for three different short exposure times (15 s, 20 s and 30 s). Regardless to the exposure time the damage done to the surface of the target material is always plastic deformation for such sort exposures.

By increasing the exposure time up to 20 s and 30 s, all characteristic features observed after 15 s are still present although the damage got more pronounced, which leads to wider and deeper holes and an increase in the measured surface roughness, eventually. Note that the jet velocity was smaller when exposing the sample for 30 s (see Table 1 for the details), therefore we did not observe a significant difference between the samples treated for 20 s and 30 s.

The reason for this is that the jet velocity plays an important role. However, to investigate the effect of these working conditions longer exposure times are needed, which was investigated in our previous publication [18].

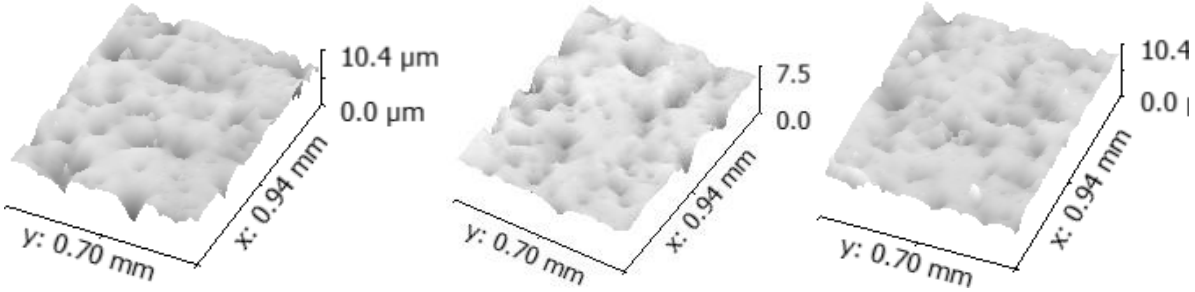

Figure 4. Surface topography of the Al- alloy sample after short time exposure (15 s, 20 s, and 30 s from left to right respectively) at 1.5 mm away from the center of jet impact (10x magnification).

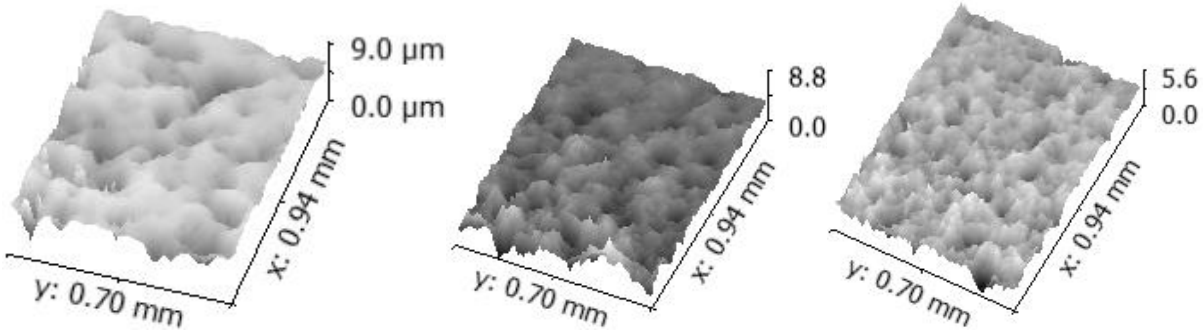

Figure 5. Surface topography of three samples (from left to right Al- alloy, Cu and SS316) after plastic deformation at 3 mm away from the center of jet impact. The exposure times were 15 s (Al-alloy), 15 s (Cu) and 1800 s (SS316), respectively (10x magnification).

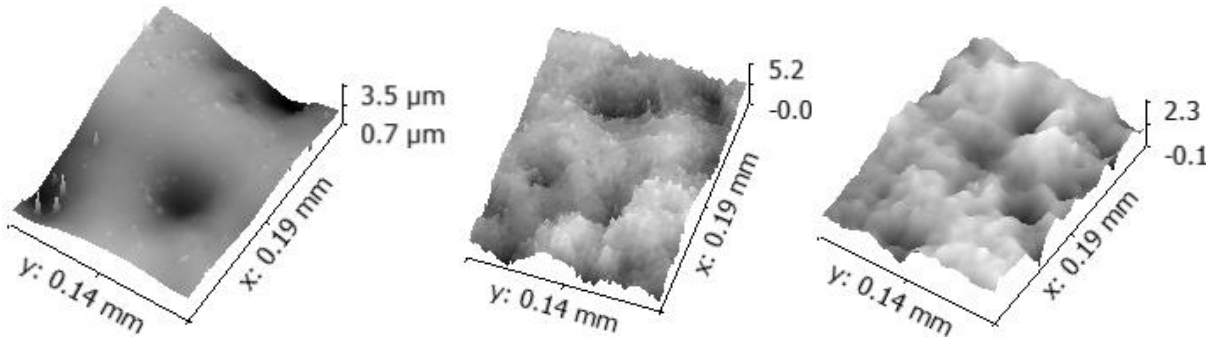

Figure 6. Surface topography of three samples (from left to right AlSiMg alloy, Cu and steel) after plastic deformation. The exposure times were 15 s (AlSiMg), 15 s (Cu) and 1800 s (steel). The position of measurements were 3 mm (AlSiMg), 0 mm (Cu) and 3 mm (Steel) away from the center of jet impact, respectively (50x magnification).

Table 2 presents numerical results measured at different spots on the surfaces. It can be concluded that 1) although the nature of the damage done to the surface is plastic deformation and thus we have the same characteristic structures for the three treated Al-alloy samples, the surface roughness increases with the exposure time; 2) the plastic deformation caused by the cavitation damage increased the surface roughness of the samples around 9 times after 15 s exposure and around 25 times after 20 s exposure (calculated at the areas of highest roughness on the treated surfaces). The measured negative skewness confirms that the dominant features on the surfaces are holes for the treated samples, while in the case of the reference samples before cavitation, the negative skewness can be attributed to the scratches on the surface after polishing. This can also be seen in Fig. 7, which presents cross-sectional profiles from the sample surfaces obtained on the images of Fig. 4.

The characteristic sizes of the features (holes) are in the 100 µm range laterally, while in the Z dimension they range several microns. That is the reason why the more convenient interferometer was used to characterize the surface roughness statistically, while AFM and EFM could only be used to examine single features (with a maximum scan range of 100 µm).

It is important to point out that the deformed surface topography is not homogenous; the roughness has a distribution, which is (quite like the circles in the illustration of Fig. 3) circularly symmetric on the point of jet impact. The distribution of the surface roughness is characterized along three axes in six measurement points per axis; this can be seen in Fig. 6 for three investigated samples.

Table 2. Surface properties (surface roughness (S_a, S_{RMS}) and skewness (S_{sk})) of the samples measured with white light interferometry. The scan size of the images, which was used for the evaluation was 0.7 mm x 0.94 mm. An average of six measurements on different areas are presented, with standard deviations, except stainless steel, where only one measurement was done per area (marked with a star (*)).

Tested materials	Measurement position away from the center of jet impact (mm)	S_a (μm)	S_{RMS} (μm)	S_{sk}
Al-alloy	Reference values, before the cavitation treatment (Exp. time = 0.0 s)	0.04 (0.01)	0.06 (0.03)	-1.29 (0.62)
Cu		0.06 (0.02)	0.09 (0.03)	-0.99 (0.56)
SS316		0.03 (0.02)	0.05 (0.03)	-1.92 (1.03)
Al-alloy (Exp. time = 15 s)	0	0.36 (0.05)	0.55 (0.03)	-1.66 (0.44)
	2	0.37 (0.03)	0.48 (0.04)	-1.77 (0.52)
	4	0.12 (0.03)	0.23 (0.04)	-0.9 (0.83)
Al-alloy (Exp. time = 20 s)	0	0.43 (0.01)	0.64 (0.03)	-1.6 (0.62)
	3	1.03 (0.07)	1.4 (0.13)	-1.28 (0.26)
	6	0.14 (0.06)	0.14 (0.11)	-3.41 (0.81)
Cu (Exp. time = 15 s)	0	1.04 (0.13)	1.4 (0.25)	-0.48 (0.08)
	2	2.87 (0.58)	3.75 (0.74)	0.07 (0.18)
	4	0.22 (0.05)	0.47 (0.2)	-1.5 (0.35)
SS316 * (Exp. time = 1800 s)	0	0.81	0.99	-0.29
	2	0.44	0.57	-0.02
	3	0.32	0.42	-0.83
	6	0.11	0.15	-1.09

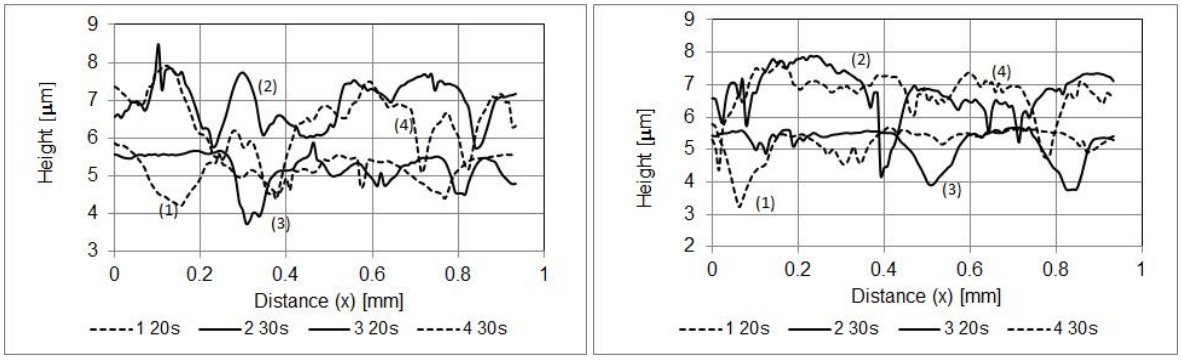

Figure 7. Cross-sectional profiles extracted from the surface topographies presented in Fig 4 for the Al-alloy sample after 20 s and 30 s exposure times. The four profiles per sample were made at positions 0.1, 0.2, 0.35 and 0.5 mm measured from the bottom of the image, respectively.

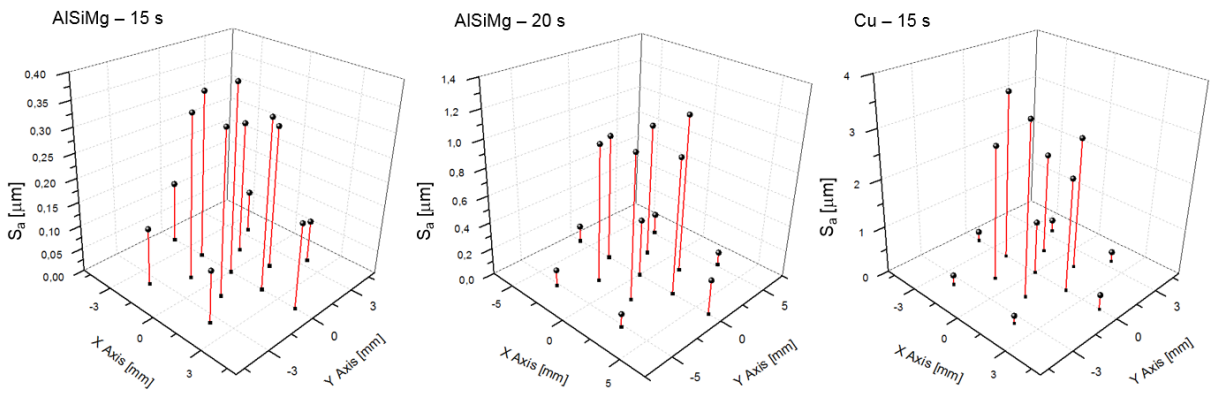

Figure 8. The distribution of surface roughness along the surface of the treated samples. The values were obtained by white light interferometry measurements on areas with a scan size of 0.7 mm x 0.94 mm. The exact measurement positions are also indicated in Table 2.

Fig. 5 compares the plastic deformation effect of cavitation on the three different investigated materials. The Al-alloy and the Cu samples were exposed for 15 s, while the steel was treated for 1800 s. The most noticeable difference between the surfaces are, that copper and steel has smaller, but more densely packed holes compared to Al- alloy. The edges of the features are also rougher in the cases of Cu and SS316, as can also be seen in Fig 6, which presents higher magnification images from the same surfaces. Based on the numerical values of Table 2 we can say that the surface roughness of copper is significantly higher compared to Al-alloy or SS316, which is 48 times higher than the reference. Copper and SS316 also has negative skewness, however, the smaller absolute values indicate that the distribution of peaks and holes are more balanced compared to Al-alloy, which is a notable difference, regarding the characteristic surface structures. By increasing the exposure time, the damage done by cavitation can move beyond plastic deformation. Erosion may occur which removes material from the sample surface. This can be observed in Fig. 3 for the Al-alloy and Cu samples after 1800 s treatment. However, studying the effect of erosion on the surface topology is beyond the scope of our current paper.

5.2.EFM Results

Electrostatic force microscopy (EFM) measurements were done on the specimens to investigate the effect of the increased surface roughness on the electrostatic field of the surface. During EFM an electrically conductive AFM tip – Si or SiN covered with a conductive material such as platinum-iridium – is electrically biased against the sample, while also oscillated in non-contact (or tapping mode) above the surface. In the case of lift mode the tip passes two times over each scanned row. During the first pass, the topography is obtained (standard tapping mode), while during the second pass the tip is lifted up to a given fixed distance from the surface, taking into consideration the previously measured topography in that row. During the second pass only the electrostatic forces between the tip and the sample surface modulate the oscillation of the tip. The electrostatic forces (F_{el}) between the tip and the surface can be expressed as in Equ.4. Note that the potential V contains not only the bias potential, but the differences in the work functions of the applied materials as well. In EFM the electrostatic forces affect the oscillation of the tip, so they modulate the tapping amplitude and phase signals, which are generally used for representation.

$$F_{el} = \frac{1}{2}\frac{\partial C}{\partial z}\Delta V^2 \qquad (4)$$

EFM is most commonly used to measure different material properties or embedded charges in the surface. The sharpest contrast in the electrostatic force map can be achieved on surfaces which for example contain both conductive and insulating parts, which contain embedded charges, or which has electrically biased parts. However, in the case of materially homogenous and conductive samples, we can presume that the changes in the measured electrostatic map entirely originate from the surface

roughness and its effect on the electrical near field of the surface. In our investigations 500 mV bias potential between the tip and the surface was applied to investigate the electrical near field at 20 nm above the sample surface.

The results for stainless steel are presented in Fig. 9. On the left side the electrostatic map (based on the EFM tapping amplitude) can be seen, which refers to the reference area (polished surface before cavitation) and topography presented in Fig. 2. The other two maps present the topography and EFM signals after 1800 s cavitation treatment. It can be seen, that the EFM map correlates with the topography (as expected for this material), but the scale of the tapping amplitude (which in this case represents the electrostatic forces) are around 4 times higher than the reference. This can be attributed to the sharp features caused by cavitation, which perturb the electric near filed above the sample. The increase in the EFM signal is also present for the other materials: the increase in the surface roughness resulted in increased EFM signals which can be even orders of magnitude higher that the reference, depending on the material properties and roughness, as can be seen in the numerical results of Table 3. Note that besides the variation in surface roughness the EFM signal can also depend on possible surface contamination, surface oxide, or material composition. The purpose of the table is to illustrate the effect of surface roughness, and not to compare the three materials with each other in terms of EFM signal. Such intensive near fields could be desirable for some applications [11-17].

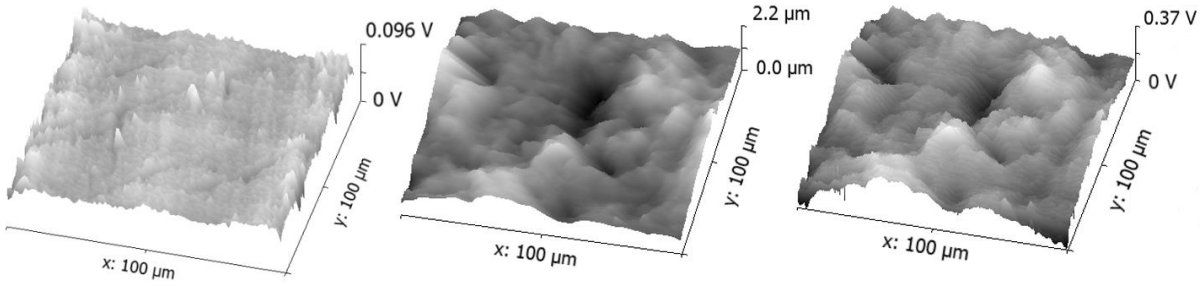

Figure 9. Electrostatic Force Microscopy (EFM) results on the SS316 sample. Left: before cavitation EFM amplitude map (the corresponding topography can be seen on Fig. 2); middle: topography after 1800 s exposure to cavitation; right: corresponding EFM amplitude map.

Table 3. AFM topography and EFM tapping signals (amplitude and phase) for three materials before and after cavitation treatment. The values are measured on images with 100 µm x 100 µm scan size.

Tested materials and exposure time	Topography			EFM tapping ampl.	EFM tapping phase
	min-max [nm]	S_a [nm]	S_{RMS} [nm]	min-max [V]	min-max [V]
Al-alloy reference (0 s)	400	16.7	22.2	0.073	0.08
Al-alloy (15 s)	1300	112	154	8	21.4
Cu reference (0 s)	208	26	33.8	2.4	3.7
Cu (15 s)	4090	459	590	4.8	20
SS316 reference (0 s)	280	15.3	20.4	0.096	1.1
SS316 (1800 s)	1200	203	245	0.37	2.6

5.3 Cavitation Damage and Material Properties

In order to establish the influence of the cavitation damage on the selected target materials three FCC materials – Al-alloy, Cu and SS316 were tested. At the beginning of cavitation attack, the virgin specimens are assumed to have smooth surfaces except to some scratches, with depths in the range of 0.1 μm, based on the AFM images of Fig. 2.

The damage done by the cavitation can be separated to different phases. First plastic deformation of the material takes place, which is followed by erosion/rupture of the surface, depending on the material properties and the exposure time. As can be seen on the optical microscopy images of Fig. 3, the damage features caused by cavitation are always concentric on the point of jet impact, and it is also possible that areas of plastic deformation and erosion follow each other along the radius. This feature can be associated with the density of the collapsing bubbles on the surface and it is governed by the nozzle geometry [18].

During the first stage of the treatment, collapsing cavitation bubbles crash on the specimen surface, which cause shock waves and work hardening at the point of impact. The work hardening, which is dominated by dislocation of forest interaction type, causes plastic deformation on the surface thereby creating a compressive layer which impedes the initiation of fatigue cracks and/or crack propagation [4]. Also, the possible influence of temperature increase during the collapse of cavitation bubbles on the damage process should be taken into account [6]. During this initial stage of cavitation damage, the surface strain increases from zero up to the strains corresponding to range between Yield Stress (YS = 320 MPa) and Ultimate Tensile Strength (UTS ≈ 370 MPa) for the Al-alloy. These values for Cu and SS316 are 150 MPa/250 MPa and 310 MPa/500 MPa, respectively. Plastic deformation occurs when the maximum stress applied on the target material is close to the threshold value near to UTS. The time which the material can sustain under this stage of damage is called the incubation time. This time is the function of the mechanical properties of the material subjected to this stress (cavitation) and the working conditions. The plastic deformation is followed by erosion, which occurs only at local areas first, so the ability of the material to absorb impact work through local coordination deformation appears to be more important [24].

The characteristic damages on the surface after plastic deformation are holes and pits, as can be seen on the presented interferometric topography results (Figures 4, 5, 6). These pits have conical shape with different inclinations, which is related to the angle of attack between the micro jet and the target surface. By extracting and evaluating the roughness profiles (as can be seen on in Fig. 7), the accurate dimensions of the pit geometry (depth, shape, surface area, etc.) can be measured. These parameters are depending on the micro-jet velocity, micro-jet diameter and the angle of attack between the jet and the target [25]. Due to the high frequency of bubble collapse on the surface, even after short exposure times, the pit volume and shape cannot be directly related to single impacts.

The irregular shape and asymmetric features of the hollows indicate that subsequent rebounds can implode over or near a crater which was previously produced by an earlier collapse and extend the impingement damage [26]. So these features are caused by collective collapses and are common in the materials-cavitation resistance tests using cavitating jets [27]. Collective collapses are typically characterized by cascades of implosions. The pressure wave emitted by the collapse and rebound of a particular bubble tends to enhance the collapse velocities of the surrounding bubbles, thus increasing the amplitude of their own pressure waves. Also the angle of impact between the wall surface and the micro-jets is not 90^{o} in most of time. The existence of collective collapses is an evidence for the existence of different angles of attack.

This process can clearly be observed through the obtained numerical values of Table 2. For example, in the case of Al alloy with low exposure times the dominant structures which define the surface roughness are holes, which reflect the collapse of individual bubbles. This can clearly be seen in the large negative skewness values, which indicate an “unbalanced” roughness, in other words a flat surface with some holes in it. In the case of steel with increased exposure times (note that steel require longer exposure times to be able to plastically deform it with cavitation) the surface roughness is higher but more balanced (“hills and holes”, indicated by a smaller absolute skewness), which clearly reflects the effect of multiple, consecutive bubble collapses on the surface.

By increasing the exposure time the surface roughness can be increased, however, based on our results on the Al-alloy sample after 15 s, 20 s and 30 s exposure times, and also on our previous

results, we can assume that a significant role can be attributed to the jet velocity (repetition of impact, i.e. the frequency of bubble generation and the frequency of collapse on the surface) [19,29].
The analysis of the results and the comparison between the three different materials suggest that the main behavior of the materials is the same. They undergo the same deformation mechanism (i.e. from initial plastic deformation to subsequent erosion/rupture), however, the exposure time to reach the subsequent stages are different. This behavior can be attributed to the differences in stacking fault energy (the distance between partial dislocations) and base strength. In copper (the highest SFE and lowest strength), the plastic deformation preceding the erosion takes place very easy, which leads to a very short incubation period and subsequent introduction of severe erosion damage even after very short exposure times. This can also be seen in the numerical results of Table 2. After 15 s exposure copper has higher surface roughness and smaller absolute skewness compared to the Al alloy, which indicates a more developed process with more pronounced damage caused by multiple bubble impingements. On the other hand, due to its lowest SFE and highest strength, stainless steel shows the characteristic of plastic deformation even after 1800 seconds of exposure. The aluminum alloy performs between the other two materials, but much closer to copper. The high negative skewness and moderate roughness indicates the first phase of plastic deformation after 15 to 30 s exposure with distinguishable bubble collapse sites (holes) on the surface. More details about the mechanism of cavitation damage and the interaction between the bubble collapse and surface of the target materials are presented in our previous publications [18, 30].

Based on the results presented in Figures 4, 5, 6 and 9 we can deduce that the cavitating jet generator could be used to evaluate some mechanical properties of components such as compression and erosion resistance from miniature-sized specimens. As well known the traditional destructive testing methods require large specimens in most of the time. However it could be a problem to obtain such large samples from a component in service without violating the structural integrity. Consequently, various non-destructive or miniaturized specimen testing techniques have been developed over the past two decades, for example the miniature tensile and shear punch techniques. The cavitating jet method has many advantages over other methods used for materials testing. The apparatus is small (both miniaturized and large specimens can be tested, by focusing the treatment on the large specimens by the adjustment of the hydrodynamic and geometrical conditions), the testing time can easily be adjusted by choosing the suitable working conditions and the results can then be scaled up or down provided the cavitation number is kept constant. However, the greatest advantage of this method is the fact that the flow parameters can be controlled independently [29].

Conclusions:

In this work we investigated the effect of cavitation damage on three different FCC materials with white light interferometry and atomic/electrostatic force microscopy. The samples were exposed to different hydrodynamic conditions for various times, and the modified topography was studied concentrating primarily on the plastic deformation phase. We demonstrated that by regulating the above conditions the surface roughness of the materials can be increased and controlled in a wide range for the tested materials. The process of plastic deformation, the interaction between the micro jet and the sample surface was discussed in accordance with the obtained numerical results. We also demonstrated that along with the increased surface roughness the electrostatic field measured above a biased sample can also be increased, accordingly. Therefore, the possibility to utilize the cavitation phenomenon as a tool, to modify the surface properties in the nano- and micro scale is illustrated extensively. Also we discussed the possible use of cavitation as a miniaturized testing method to evaluate some mechanical properties of components which have small dimensions, and to identify their behavior caused by the size dependence.

References:

1 Rayleigh, L., 1917, VIII On the pressure developed in a liquid during the collapse of a spherical

cavity. Philosophical Magazine Series 6, 34, 94–98. doi:10.1080/14786440808635681. ISSN 1941-5982.
2 Christopher, E.B., 1995, Cavitation and Bubble Dynamics, by Oxford University Press, ISBN 0-19-509409-3, Chapter 1-4. http://caltechbook.library.caltech.edu/1/4/bubble.htm
3 Soyama, H., et al., 2002, Improvement of Fatigue Strength of Al-Alloy by Cavitation Shot-Less Peening, Transactions of the ASME, Journal of Engineering Materials and Technology,124, 2:135-139.
4 Soyama, H., 2007, Improvement of Fatigue Strength by Using Cavitating Jets in Air and Water, Journal of Materials Science, 42, 16:6638-6641.
5 Abdolreza, D., Ahmad, N., 2005, Modern Trends in Detection of Cavitation Erosion in Hydro Power Plants, 20th International Power System Conference. http://www.krec.ir/confferance/20/proceedings/98-E-EPG-850.pdf
6 Knapp, R.T., et al., 1970, Cavitations, McGraw-Hill, Chapter 1-8
7 Regiane, F.P., et al., 2000, Cavitation Damage Measurement by 3D Laser Profilometry, Wear, 246, 59–67.
8 Thomas, T.R., 1998, Trends in Surface Roughness, International Journal of Machine Tools and Manufacture, 38, 405-411.
9 Jakson, M.J., Ahmed, W., 2007, Surface Engineering Surgical Tools and Medical Devices, Springer, ISBN: 97B-0-387-27026-5, 21-47. http://www.springer.com/engineering/biomedical+engineering/book/978-0-387-27026-5
10 Bahrami, M., et al., 2004, Thermal Contact Resistance of Nonconforming Rough Surfaces, Part 2: Thermal Model, Journal of Thermophysics and Heat Transfer, 18, 218-227.
11 Lazić, P., Persson, B.N.J., 2010, Surface-Roughness–Induced Electric-Field Enhancement And Triboluminescence, Europhysics Letters, 9, 460003p1-46003p5,doi:10.1209/0295-5075 /91 /46003.
12 John, H.B., 2008, Plasma Physics and Related Challenges of Millimeter-Wave-to-Terahertz and High Power Microwave Generation, Physics of Plasmas, 15, 055502-1-16.
13 Pandit, H., et al., 2005, High Tc Superconductor Re-Entrant Cavity Filter Structures Physica C: Superconductivity and its applications, 425, 44-51, DOI:10.1016/j.physc.2005.05.010.
14 Peng, Z., et al., 2009, Analysis of Radio-Frequency Absorption and Electric and Magnetic Field Enhancements Due to Surface Roughness, Journal of Applied Physics, 105, 114908-1-1149088.
15 Caughman, J., et al., 2007, Study of RF Breakdown Mechanisms Relevant To An ICH Antenna Environment, Radio Frequency Power In Plasmas: 17th Topical Conference On Radio Frequency Power In Plasmas. AIP Conference Proceedings, 933, 195-202.
16 Kevin, L.J., 2008, Electron Emission Contributions to Dark Current and Its Relation to Microscopic Field Enhancement and Heating in Accelerator Structures, Physical Review Special Topics - Accelerators and Beams, 11, 081001-1- 081001-17.
17 Vasil'ev, A.A., 2005, Use of Superconducting RF Systems in Low-Energy Accelerators**,** Atomic Energy, 99, 730-734
18 Hutli, E., et al., 2008, Mechanics of Submerged Jet Cavitating Action: Material Properties, Exposure Time and Temperature Effects on Erosion, Archive of Applied Mechanics, 78, 329-341.
19 Hutli, E., et al., 2012, New Method to Determine Shedding/Discharging Frequency of Cavitation Clouds Based on Computer Tomography,15th International Conference on Fluid Flow Technologies- Budapest, Hungary.
20 Hutli, E., et al., 2013, Influences of Hydrodynamic Conditions, Nozzle Geometry on Appearance of High Submerged Cavitating Jets, THERMAL SCIENCE, 17, 1139-1149
21 Hirox-Digital Microscope KH-770 **http://www.hiroxusa.com/products/microscope/kh7700_02.html**
22 Zygo: NewView 7100 Operating Manual, Zygo Corporation (Laurel Brook Road, Middlefield, CT 06455, USA)
23 Bruker AFM Probes Americas, http://www.brukerafmprobes.com/p-3392-scm-pit.aspx
24 Wenge, C., et al., 2006, Correlation of Cavitation Erosion Resistance and Mechanical Properties of Some Engineering Steels, Journal of Materials Science- Letters, 41, 2151-2153.
25 Chen, H.S., et al., 2008, Effect of Hydrodynamic Pressures near Solid Surfaces in the

Incubation Stage of Cavitation Erosion, Proceedings of the Institution of Mechanical Engineers, Journal of Engineering Tribology, 222, 523-531.

26 Ayat, K., 1987, Cavitation Erosion of a Duplex Stainless Steel, Materials Science and Engineering, 86, 191-203.

27 Jean, P.F., Jean, M.M., 2006, Fluid Mechanics and Its Applications ISSN 0926-5112, Fundamentals of Cavitation, chapter12-Cavitation erosion, 76, 265-291 http://www.springerlink.com/content/p6263wk52850768v/?p=8c41a8b1f47a444c90e735a1249d61&pi=11

28 Brunton, J.H., 1966, High Speed Liquid Impact, Philosophical Transactions of the Royal Society of London. Series A, Mathematical and Physical Sciences, the Royal Society,79-85.

29 Hutli, E., Nedeljkovic, M., 2008, Frequency in Shedding/Discharging Cavitation Clouds Determined by Visualization of a Submerged Cavitating Jet, Journal of Fluids Engineering, Transaction of the ASME, 130, 561-568

30 Hutli, E., et al., 2013, Nano- and Micro-Scale Surface Modification of FCC Metal Using High Submerged Cavitating Water Jet, Plasmonics,8, 8:843–849, DOI 10.1007/s11468-013-9481-6